2008

Predictive Control of a Munition Using Low-Speed Linear Theory

Nathan Slegers

George Fox University, nslegers@georgefox.edu

Predictive Control of a Munition Using Low-Speed Linear Theory

Nathan Slegers*
University of Alabama in Huntsville, Huntsville, Alabama 35899

Nomenclature

A, B, C, E, F, G, H, K	=	longitudinal and lateral equation coefficients
C_{DD}	=	fin cant rolling aerodynamic coefficient
C_{LL}, C_{MM}, C_{NN}	=	roll, pitch, and yaw control aerodynamic coefficients
C_{LP}, C_{MQ}, C_{NR}	=	roll, pitch, and yaw damping aerodynamic coefficients
$C_{\max}$	=	pitch and yaw control limit
C_{NA}	=	normal force aerodynamic coefficient
C_{x0}	=	zero yaw drag aerodynamic coefficient
C_{x2}	=	yaw squared drag aerodynamic coefficient
D	=	reference diameter
$\mathbf{e}$	=	impact-error vector
$e_{\max}$	=	impact-error stopping criterion
g	=	gravitational constant
I	=	munition inertia matrix
I_{XX}, I_{YY}, I_{ZZ}	=	moments of inertia
I_{XY}, I_{YZ}, I_{XZ}	=	products of inertia
K	=	predictive control gain matrix
$k_{\max}$	=	control iteration limit
$\tilde{L}, \tilde{M}, \tilde{N}$	=	external moments in the nonrolling frame
$\tilde{L}_A, \tilde{M}_A, \tilde{N}_A$	=	aerodynamic moments in the nonrolling frame
$\tilde{L}_C, \tilde{M}_C, \tilde{N}_C$	=	control moments in the nonrolling frame
$\tilde{L}_{\mathrm{UA}}, \tilde{M}_{\mathrm{UA}}, \tilde{N}_{\mathrm{UA}}$	=	unsteady aerodynamic moments in the nonrolling frame
m	=	mass
$\tilde{p}, \tilde{q}, \tilde{r}$	=	angular velocity components in the nonrolling frame
$R_{\oplus AX}$	=	distance from the mass center to the aerodynamic center along the station line.
s	=	nondimensional arc length
$\tilde{u}, \tilde{v}, \tilde{w}$	=	velocity components in the nonrolling frame
$\tilde{u}_w, \tilde{v}_w, \tilde{w}_w$	=	wind velocity components in the nonrolling frame
V	=	total velocity
V_x, V_z	=	longitudinal velocity components
$\tilde{w}_0, \tilde{q}_0, \theta_0$	=	vertical velocity, pitch rate, and pitch in nonrolling frame at the beginning of an update interval
x, y, z	=	inertial positions of the mass center
$\tilde{X}, \tilde{Y}, \tilde{Z}$	=	external forces in the nonrolling frame
$\tilde{X}_A, \tilde{Y}_A, \tilde{Z}_A$	=	aerodynamic forces in the nonrolling frame
$\tilde{X}_W, \tilde{Y}_W, Z_W$	=	weight in the nonrolling frame
x_I, y_I, z_I	=	predicted-impact position components
x_T, y_T, z_T	=	target position components
α, β	=	aerodynamic angle of attack and side slip
$\lambda, \sigma_1, \Phi_1$	=	longitudinal equation's pole, real, and imaginary components
ρ	=	atmospheric density
σ_2, Φ_2	=	lateral equation's real and imaginary components
$\phi, \theta,$	=	Euler roll, pitch, and yaw angles

*Assistant Professor, Department of Mechanical and Aerospace Engineering. Member AIAA.

I. Introduction

EXISTING tactical unmanned aerial systems (UAS) provide improved capability in performing a diverse set of military missions such as reconnaissance and targeting. The potential of tactical UAS is impressive, yet use on the battlefield is limited because existing UAS have no capability to engage a time-critical identified target. One solution is to add small munitions that can be released by the UAS. Adding weaponized payloads to existing UAS is limited by many practical issues. The small payload capabilities of existing systems require the munitions to be small, lightweight, and easily integrated into existing platforms. To be effectively integrated into a UAS mission, the munition must be allowed to be released from a general area. A practical system would receive only target information, initial states, and a release command. The munition would then be required to compensate for errors in release position, velocity, and orientation during its trajectory. Possible solutions include existing 40- and 60-mm munitions with modified tail sections for guidance, stability, and control. A small blast radius requires the small munitions to have guidance to reduce dispersion induced from release.

Guidance techniques for munitions are well established, with details on many standard control techniques provided by Zarchan [1]. Alternative control techniques have also been investigated, such as pulse jets on a spinning projectile using proportional navigation [2]. Later, Jitpraphai and Costello [3] also investigated pulse jets for trajectory tracking of direct-fire rockets. More recently, dynamic inversion with neural networks and control Lyapunov functions have been used for guided munitions [4,5].

The work reported here develops a predictive guidance strategy to reduce dispersion of a small statically stable munition using tail surfaces for control. Predictive control uses a dynamic model to predict the future state, which is then used to determine suitable control. Model predictive control has been successfully applied over a range of systems such as guided parafoils and unmanned systems [6,7]. Model predictive control has also been successfully applied to projectiles by Burchett and Costello [8]. They investigated pulse jets located near the nose on a slow-spinning fin-stabilized rocket with pulse-jet firing logic based on a projectile linear model. Ollerenshaw and Costello [9] later applied projectile linear theory to a canard-

controlled projectile and formed an optimal predictive control solution. In both cases, the authors employed a set of assumptions such as small aerodynamic angles, large roll rate compared with pitch and yaw rates, and near-flat-fire conditions, resulting in a set of analytically solvable equations commonly referred to as projectile linear theory [10]. Conventional projectile linear theory has been extended to account for various specialized cases such as fluid payloads [11], lateral impulses [12], and dual-spin projectiles [13]. Recently, Hainz and Costello [14] developed a modified linear theory that accounts for large pitch while retaining the small-aerodynamic-angle assumption of conventional linear theory.

A munition released at low speeds provides unique problems for projectile linear theory, because pitch ranges from near zero at release to near vertical at impact and vertical velocities and pitch rates may become significant. Modified linear theory accounts for the former, but large impact-prediction error occurs due to influence of vertical velocities and pitch rates during prediction of yaw, pitch, and total velocity. This work considers a statically stable low-speed munition with low spin rate. Modified linear theory is changed to account for vertical velocities, pitch rates, and control surfaces to improve impact prediction. Furthermore, the roll rate is considered small, resulting in separation of the epicyclic equations into longitudinal and lateral equations. Low-speed modified linear theory is used to rapidly compute impact predictions that are fed to the guidance system. The guidance system uses tail control surfaces to reduce the predicted-impact errors. Simulations are used to demonstrate the effective dispersion reduction of the predictive control strategy.

II. Dynamic Model

A munition can be modeled as a rigid body possessing six degrees of freedom (6DOF), including three inertial position components of the system mass center as well as the three Euler orientation angles, as shown in Fig. 1. A body reference frame is fixed to the body, where I_B is aligned with the axis of revolution. A nonrolling frame with I_N, also aligned with the axis of revolution, is defined so that it is fixed to the body but does not roll. The dynamic equations of motion are derived in the nonrolling frame and provided in Eqs. (1–4).

$$\begin{Bmatrix} \dot{x} \\ \dot{y} \\ \dot{z} \end{Bmatrix} = \begin{bmatrix} c_\theta c & -s & s_\theta c \\ c_\theta s & c & s_\theta s \\ -s_\theta & 0 & c_\theta \end{bmatrix} \begin{Bmatrix} \tilde{u} \\ \tilde{v} \\ \tilde{w} \end{Bmatrix} \tag{1}$$

$$\begin{Bmatrix} \dot{\phi} \\ \dot{\theta} \\ \dot{\psi} \end{Bmatrix} = \begin{bmatrix} 1 & 0 & t_\theta \\ 0 & 1 & 0 \\ 0 & 0 & 1/c_\theta \end{bmatrix} \begin{Bmatrix} \tilde{p} \\ \tilde{q} \\ \tilde{r} \end{Bmatrix} \tag{2}$$

$$\begin{Bmatrix} \dot{\tilde{u}} \\ \dot{\tilde{v}} \\ \dot{\tilde{w}} \end{Bmatrix} = \frac{1}{m} \begin{Bmatrix} \tilde{X} \\ \tilde{Y} \\ \tilde{Z} \end{Bmatrix} + \begin{Bmatrix} \tilde{r}\,\tilde{v} - \tilde{q}\,\tilde{w} \\ -t_\theta \tilde{r}\,\tilde{w} - \tilde{r}\,\tilde{u} \\ \tilde{q}\,\tilde{u} + t_\theta \tilde{r}\,\tilde{v} \end{Bmatrix} \tag{3}$$

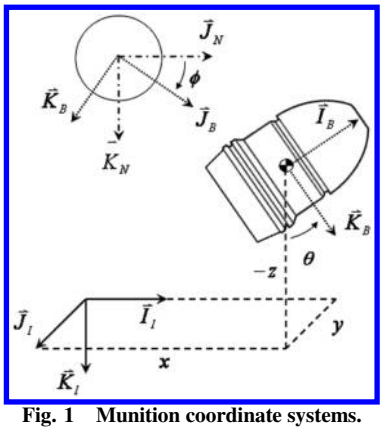

Fig. 1 Munition coordinate systems.

$$\begin{Bmatrix} \dot{\tilde{p}} \\ \dot{\tilde{q}} \\ \dot{\tilde{r}} \end{Bmatrix} = [I]^{-1} \left(\begin{Bmatrix} \tilde{L} \\ \tilde{M} \\ \tilde{N} \end{Bmatrix} - \begin{bmatrix} 0 & -\tilde{r} & \tilde{q} \\ \tilde{r} & 0 & t_\theta \tilde{r} \\ -\tilde{q} & -t_\theta \tilde{r} & 0 \end{bmatrix} [I] \begin{Bmatrix} \tilde{p} \\ \tilde{q} \\ \tilde{r} \end{Bmatrix} \right) \tag{4}$$

In Eqs. (1–4), the common notations $\sin(\alpha) \equiv s_\alpha$, $\cos(\alpha) \equiv s_\alpha$ and $\tan(\alpha) \equiv t_\alpha$ are used. Forces appearing in the previous equations have contributions from weight and aerodynamic loads with Magnus forces neglected because of the munition's slow spin rates. The combined forces are provided in Eq. (5).

$$\begin{Bmatrix} \tilde{X} \\ \tilde{Y} \\ \tilde{Z} \end{Bmatrix} = \begin{Bmatrix} \tilde{X}_W \\ \tilde{Y}_W \\ \tilde{Z}_W \end{Bmatrix} + \begin{Bmatrix} \tilde{X}_A \\ \tilde{Y}_A \\ \tilde{Z}_A \end{Bmatrix} \tag{5}$$

Weight and aerodynamic forces in a nonrolling reference frame are given in Eqs. (6) and (7), with aerodynamic angles defined in Eqs. (8) and (9).

$$\begin{Bmatrix} \tilde{X}_W \\ \tilde{Y}_W \\ \tilde{Z}_W \end{Bmatrix} = mg \begin{Bmatrix} -s_\theta \\ 0 \\ c_\theta \end{Bmatrix} \tag{6}$$

$$\begin{Bmatrix} \tilde{X}_A \\ \tilde{Y}_A \\ \tilde{Z}_A \end{Bmatrix} = -\frac{\pi}{8} \rho V^2 D^2 \begin{Bmatrix} C_{x0} + C_{x2}(\alpha^2 + \beta^2) \\ C_{\mathrm{NA}} \beta \\ C_{\mathrm{NA}} \alpha \end{Bmatrix} \tag{7}$$

$$\alpha = \tan^{-1}((\tilde{w} - \tilde{w}_w)/(\tilde{u} - \tilde{u}_w)) \tag{8}$$

$$\beta = \tan^{-1}((\tilde{v} - \tilde{v}_w)/(\tilde{u} - \tilde{u}_w)) \tag{9}$$

Moments acting on the munition have contributions form aerodynamic forces, unsteady aerodynamic moments, and control moments.

$$\begin{Bmatrix} \tilde{L} \\ \tilde{M} \\ \tilde{N} \end{Bmatrix} = \begin{Bmatrix} \tilde{L}_A \\ \tilde{M}_A \\ \tilde{N}_A \end{Bmatrix} + \begin{Bmatrix} \tilde{L}_{\mathrm{UA}} \\ \tilde{M}_{\mathrm{UA}} \\ \tilde{N}_{\mathrm{UA}} \end{Bmatrix} + \begin{Bmatrix} \tilde{L}_c \\ \tilde{M}_c \\ \tilde{N}_c \end{Bmatrix} \tag{10}$$

Moments due to aerodynamic forces and unsteady aerodynamic moments are

$$\begin{Bmatrix} \tilde{L}_A \\ \tilde{M}_A \\ \tilde{N}_A \end{Bmatrix} = \begin{bmatrix} 0 & 0 & 0 \\ 0 & 0 & -R_{\oplus AX} \\ 0 & R_{\oplus AX} & 0 \end{bmatrix} \begin{Bmatrix} \tilde{X}_A \\ \tilde{Y}_A \\ \tilde{Z}_A \end{Bmatrix} \tag{11}$$

$$\begin{Bmatrix} \tilde{L}_{\mathrm{UA}} \\ \tilde{M}_{\mathrm{UA}} \\ \tilde{N}_{\mathrm{UA}} \end{Bmatrix} = \frac{\pi}{8} \rho V^2 D^3 \begin{Bmatrix} C_{DD} + \tilde{p} C_{LP}(D/2V) \\ \tilde{q} C_{MQ}(D/2V) \\ \tilde{r} C_{NR}(D/2V) \end{Bmatrix} \tag{12}$$

Control is achieved through deflection of tail surfaces and is modeled as the injection of control moment coefficients.

$$\begin{Bmatrix} \tilde{L}_C \\ \tilde{M}_V \\ \tilde{N}_C \end{Bmatrix} = \frac{\pi}{8} \rho V^2 D^3 \begin{Bmatrix} C_{LL} \\ C_{MM} \\ C_{NN} \end{Bmatrix} \tag{13}$$

III. Trajectory Solution

The previous munition dynamic model is highly nonlinear and must be numerically integrated to estimate a trajectory. Historically, simplifications have been applied such as assuming symmetry, small Euler pitch and yaw angles, small aerodynamic angles of attack, velocity along the axis of revolution that is equal to the total velocity V, and a roll rate that is large when compared with pitch and yaw rates. These assumptions result in standard projectile linear theory [10], which yields accurate analytic solutions for flat-fire projectile

trajectories. In the case of large pitch angles, standard linear theory results in significant impact-prediction errors. Recently, modified linear theory has been developed by relaxing the small-Euler-pitch-angle assumption [14]. The result is a reasonably accurate analytic solution that usually requires some updates during the trajectory to account for pitch changes. Although modified linear theory addresses large pitch angles, low-speed munitions require two additional assumptions to be addressed. The vertical velocity and pitch rate may be significant and the roll rate is small. To develop suitable linear theory equations for a statically stable low-speed munition, the following assumptions are made.

1) A change of variable is made from the body velocity $\tilde{u}$ to total velocity V.

2) Velocity along the axis of revolution V is large compared with the side velocity $\tilde{v}$, $\tilde{v}_w$, and the roll and yaw rates $\tilde{p}$ and $\tilde{r}$. Higher-order terms involving $\tilde{v}$, $\tilde{v}_w$, $\tilde{p}$, and $\tilde{r}$ are neglected. Nothing is assumed about the vertical velocity $\tilde{w}$, $\tilde{w}_w$, and pitch rate $\tilde{q}$.

3) Yaw angle is small, allowing the following small-angle approximations.

$$\sin(\psi) \approx \psi, \qquad \cos(\psi) \approx 1 \tag{14}$$

4) Aerodynamic angles are small, allowing the following small-angle approximations.

$$\alpha \approx (\tilde{w} - \tilde{w}_w)/V, \qquad \beta \approx (\tilde{v} - \tilde{v}_w)/V \tag{15}$$

5) Munition is both geometrically and aerodynamically symmetric, resulting in the following simplifications.

$$I_{XY} = I_{XZ} = I_{YZ} = 0 \tag{16}$$

$$I_{YY} = I_{ZZ} \tag{17}$$

$$C_{MQ} = C_{NR} \tag{18}$$

6) Total velocity can be represented as a point mass.

$$\dot{V}_x = -\left(\frac{1}{8m}\pi\rho V D^2 C_{x0}\right) V_x \tag{19}$$

$$\dot{V}_z = -\left(\frac{1}{8m}\pi\rho V D^2 C_{x0}\right) V_z + g \tag{20}$$

$$V = \sqrt{V_x^2 + V_z^2} \tag{21}$$

7) Independent variable is changed from time t to dimensionless arc length s, measured in calibers of travel.

$$s = \frac{1}{D}\int_0^t V \, \mathrm{d}t \tag{22}$$

The common notation of a prime superscript represents a derivative with respect to dimensionless arc length s. The following relationship between the arc length and time derivatives exists.

$$\xi' = (D/V)\dot{\xi} \tag{23}$$

Application of the previous seven assumptions yields the following simplified equations.

$$x' = c_\theta D \tag{24}$$

$$y' = c_\theta D\psi + \left(\frac{D}{V}\right)\tilde{v} + \left(\frac{s_\theta \psi D}{V}\right)\tilde{w} \tag{25}$$

$$z' = -Ds_\theta + \left(\frac{Dc_\theta}{V}\right)\tilde{w} \tag{26}$$

$$\theta' = \frac{D}{V}\tilde{q} \tag{27}$$

$$\psi' = \frac{D}{Vc_\theta}\tilde{r} \tag{28}$$

$$\tilde{v}' = -\frac{\pi\rho D^3}{8m} C_{\mathrm{NA}}(\tilde{v} - \tilde{v}_w) - \left(1 + \frac{t_\theta \tilde{w}}{V}\right) D\tilde{r} \tag{29}$$

$$\tilde{w}' = -\frac{\pi\rho D^3}{8m} C_{\mathrm{NA}}(\tilde{w} - \tilde{w}_w) + D\tilde{q} + \frac{Dg}{V} c_\theta \tag{30}$$

$$\tilde{q}' = \frac{\pi\rho D^3 R_{\oplus AX}}{8I_{YY}} C_{\mathrm{NA}}(\tilde{w} - \tilde{w}_w) + \frac{\pi\rho D^5}{16 I_{YY}} C_{MQ}\tilde{q} + \frac{\pi\rho D^4 V}{8I_{YY}} C_{MM} \tag{31}$$

$$\tilde{r}' = -\frac{\pi\rho D^3 R_{\oplus AX}}{8I_{YY}} C_{\mathrm{NA}}(\tilde{v} - \tilde{v}_w) + \frac{\pi\rho D^5}{16 I_{YY}} C_{MQ}\tilde{r} + \frac{\tilde{q}_0 t_\theta D}{V}\tilde{r} + \frac{\pi\rho D^4 V}{8I_{YY}} C_{NN} \tag{32}$$

$$V_x' = -\left(\frac{1}{8m}\pi\rho D^3 C_{x0}\right) V_x \tag{33}$$

$$V_z' = -\left(\frac{1}{8m}\pi\rho D^3 C_{x0}\right) V_z + \frac{Dg}{V} \tag{34}$$

Approximate closed-form solutions can be found by making the additional assumptions that aerodynamic coefficients are constant and total velocity V is slowly changing, being treated only as a dynamic variable in Eqs. (21), (33), and (34). As with conventional and modified linear theory, these assumptions largely decouple the equations into velocity, roll rate, Euler angle, and swerve equations. A difference occurs in the epicyclic equations in which they can be further decoupled into longitudinal and lateral equations, with Euler pitch included in the former.

A. Longitudinal Solution

Expanding the cosine of Euler pitch in Eq. (30) as a first-order Taylor series and treating the total velocity V as constant, Eqs. (27), (30), and (31) can be written in the form

$$\begin{Bmatrix} \tilde{w}' \\ \tilde{q}' \\ \theta' \end{Bmatrix} = \begin{bmatrix} -A & D & B \\ C/D & E & 0 \\ 0 & D/V & 0 \end{bmatrix} \begin{Bmatrix} \tilde{w} \\ \tilde{q} \\ \theta \end{Bmatrix} + \begin{Bmatrix} G + A\tilde{w}_w \\ KC_{MM} - (C/D)\tilde{w}_w \\ 0 \end{Bmatrix} \tag{35}$$

The coefficients appearing in Eq. (35) are

$$A = (\pi\rho D^3/8m) C_{\mathrm{NA}} \tag{36}$$

$$B = -Dgs_{\theta_0}/V \tag{37}$$

$$C = (\pi\rho D^4 R_{\oplus AX}/8I_{YY}) C_{\mathrm{NA}} \tag{38}$$

$$E = (\pi\rho D^5/16I_{YY})C_{MQ} \tag{39}$$

$$G = (Dg/V)(c_{\theta_0} + s_{\theta_0}\theta_0) \tag{40}$$

$$K = (\pi\rho D^4 V/8I_{YY}) \tag{41}$$

The longitudinal eigenvalues are a simple pole λ and a complex pair $\sigma_1 \pm i\Phi_1$. Laplace transformations are used to solve the coupled differential equations in Eq. (35), with the solution shown next. Coefficients in Eqs. (42–44) are easily found by solving algebraic equations; however, they are extensive and not included. The longitudinal equations for the low-speed solution are fundamentally different from modified linear theory because of the inclusion of a decaying exponential and only one damped sinusoid.

$$\tilde{w}(s) = C_{w0} + C_{we}e^{-\lambda s} + e^{\sigma_1 s}[C_{wc}\cos(\Phi_1 s) + C_{ws}\sin(\Phi_1 s)] \tag{42}$$

$$\tilde{q}(s) = C_{q0} + C_{qe}e^{-\lambda s} + e^{\sigma_1 s}[C_{qc}\cos(\Phi_1 s) + C_{qs}\sin(\Phi_1 s)] \tag{43}$$

$$\theta(s) = C_{\theta 0} + C_{\theta e}e^{-\lambda s} + e^{\sigma_1 s}[C_{\theta c}\cos(\Phi_1 s) + C_{\theta s}\sin(\Phi_1 s)] \tag{44}$$

B. Lateral Solution

Treating the total velocity V and longitudinal states as constant, Eqs. (29) and (32) can be written in the form

$$\begin{Bmatrix} \tilde{v}' \\ \tilde{r}' \end{Bmatrix} = \begin{bmatrix} -A & -H \\ -C/D & F \end{bmatrix} \begin{Bmatrix} \tilde{v} \\ \tilde{r} \end{Bmatrix} + \begin{Bmatrix} A\tilde{v}_w \\ KC_{\mathrm{NN}} + (C/D)\tilde{v}_w \end{Bmatrix} \tag{45}$$

$$F = E + \frac{D\tilde{q}_0}{V} t_{\theta_0} \tag{46}$$

$$H = D\left(1 + \frac{t_{\theta_0}\tilde{w}_0}{V}\right) \tag{47}$$

A difference in the low-speed lateral solution and the modified linear theory lateral solution is the inclusion of the second components of the coefficients in Eqs. (46) and (47). The lateral eigenvalues are a complex pair, $\sigma_2 \pm i\Phi_2$, leading to the approximate solution in Eqs. (48) and (49). Similar to the longitudinal solution, the coefficients in Eqs. (48) and (49) are found by taking the Laplace transform of Eq. (45) and solving the resulting algebraic equations.

$$\tilde{v}(s) = C_{v0} + e^{\sigma_1 s}[C_{vc}\cos(\Phi_2 s) + C_{vs}\sin(\Phi_2 s)] \tag{48}$$

$$\tilde{r}(s) = C_{r0} + e^{\sigma_2 s}[C_{rc}\cos(\Phi_2 s) + C_{rs}\sin(\Phi_2 s)] \tag{49}$$

C. Euler Yaw and Swerve Solution

Following the same assumptions as modified linear theory, the remaining yaw and position states are simplified by treating yaw and pitch as constant when they appear with other independent variables. When Euler pitch is the only variable, its integral is approximated by the trapezoid method. Integration of Eqs. (24–26) and (28) then yields

$$\psi(s) = C_{\psi 0} + C_{\psi 1}s + e^{\sigma_2 s}[C_{\psi c}\cos(\Phi_2 s) + C_{\psi s}\sin(\Phi_2 s)] \tag{50}$$

$$x(s) = x_0 + \tfrac{1}{2}Ds[\cos[\theta(s)] + \cos[\theta_0]] \tag{51}$$

$$\begin{aligned} y(s) = {} & C_{y0} + C_{y1}s + C_{y2}s^2 + C_{ye}e^{-\lambda s} \\ & + e^{\sigma_1 s}[C_{yc1}\cos(\Phi_1 s) + C_{ys1}\sin(\Phi_1 s)] \\ & + e^{\sigma_2 s}[C_{yc2}\cos(\Phi_2 s) + C_{ys2}\sin(\Phi_2 s)] \end{aligned} \tag{52}$$

$$\begin{aligned} z(s) = {} & C_{z0} + C_{z1}s + C_{ze}e^{-\lambda s} - \tfrac{1}{2}Ds[\sin[\theta(s)] + \sin[\theta_0]] \\ & + e^{\sigma_1 s}[C_{zc}\cos(\Phi_1 s) + C_{zs}\sin(\Phi_1 s)] \end{aligned} \tag{53}$$

The inclusion of pitch in the longitudinal equations alters the cross-range and altitude equations, when compared with modified and standard linear theory, by the addition of a pure exponential decaying term. Improvements in the lateral solution also directly enter the cross-range equation, as seen in Eq. (25). Equations (42–44) and (48–53) could be used directly for trajectory generation or impact prediction. However, because of the variation of coefficients in Eqs. (35) and (45) over the trajectory, errors can become large if they are treated as constant over an entire solution. Coefficients change during the trajectory primarily for two reasons: the total velocity influencing coefficients B, G, F, and H and the changing pitch angle influencing coefficients G, F, and H. In a manner similar to standard and modified linear theory, errors can be minimized by updating the coefficients periodically over the entire trajectory.

IV. Trajectory Results

The improvements in impact prediction of low-speed linear theory over modified linear theory are highlighted using a low-speed release at 20 m/s, representing a typical loiter speed of a wide range of small UAS. Trajectories are computed using a 6DOF simulation representing the true trajectory, modified linear theory, and low-speed linear theory. The munition used in all simulations is a representative 40-mm-diam grenade with an additional theoretical tail section for static stability. Aerodynamic coefficients and physical parameters are listed in Table 1. The tail section includes four control fins that can be mixed together to produce roll, pitch, and yaw moments during guided trajectories. Both modified and low-speed linear theory use an update interval of 250 calibers, resulting in a 10-m update interval for the example munition. The 6DOF simulation is integrated using fourth-order Runge–Kutta with a time step of 0.0001 s.

Figures 2–5 show a comparison of a 6DOF simulation, modified linear theory, and the low-speed corrected modified linear theory, with no wind and the following initial conditions: $x = 0.0$ m; $y = 0.0$ m; $z = 500$ m; ϕ, θ, and $\psi = 0.0$ deg; $\tilde{u} = 50.0$ m/s; $\tilde{v} = 0.0$ m/s; $\tilde{w} = 0.0$ m/s; $\tilde{p} = 0.0$ rad/s; $\tilde{q} = -0.15$ rad/s; and $\tilde{r} = -0.15$ rad/s. Figure 2 shows the angle of attack being large with $\tilde{w}$: as large as 15% of the total velocity. In this case, the modified linear theory assumption of small $\tilde{w}$ is unacceptable and significant errors can be seen, whereas low-speed linear theory accurately predicts the angle of attack. Similar results are seen in the pitch and yaw angles shown in Fig. 3. Modified linear theory errors in $\tilde{w}$ lead to large errors in predicted pitch and yaw angles.

Table 1 Munition properties

Parameter	Value
m, kg	0.278
I_{XX}, kg · m^2	3.861×10^{-5}
I_{YY}, I_{ZZ}, kg · m^2	4.685×10^{-4}
D, m	0.04
$R_{\oplus AX}$, m	−0.0153
C_{x0}	0.309
C_{x2}	3.96
C_{NA}	4.96
C_{DD}	0.00
C_{LP}	−0.081
C_{MQ}, C_{NR}	−8.96

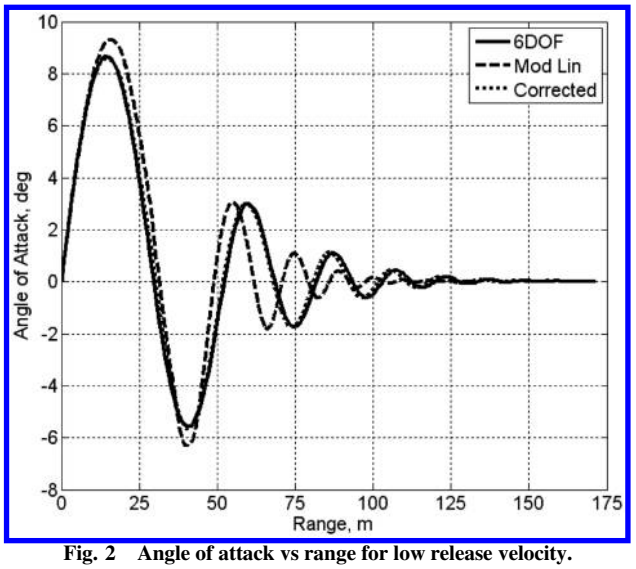

Fig. 2 Angle of attack vs range for low release velocity.

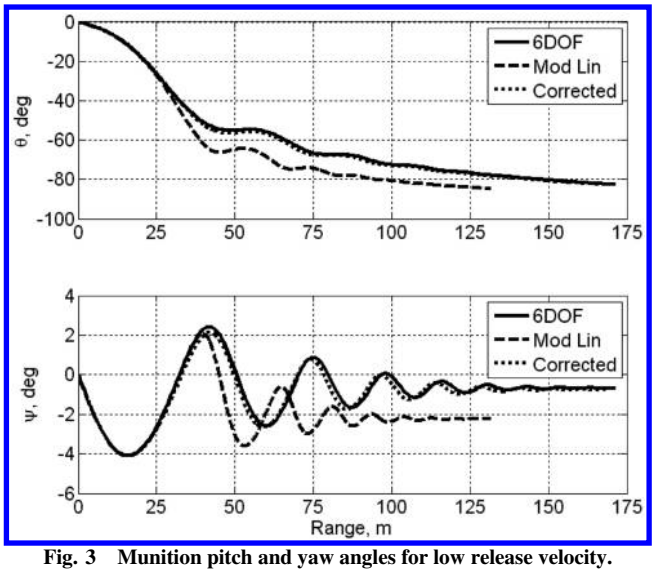

Fig. 3 Munition pitch and yaw angles for low release velocity.

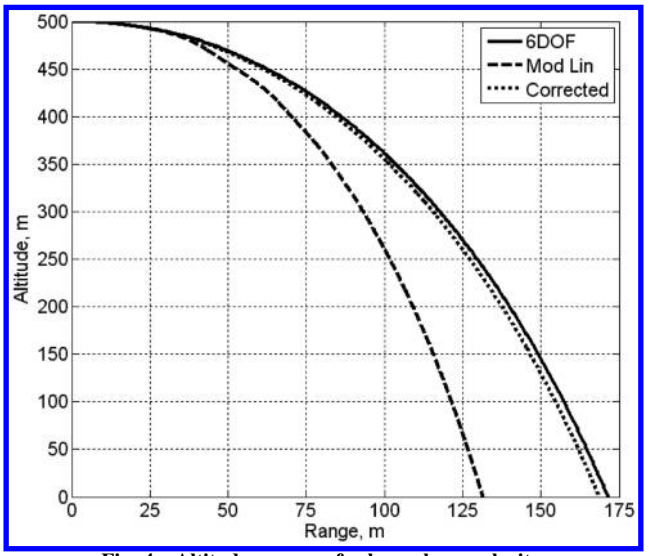

Fig. 4 Altitude vs range for low release velocity.

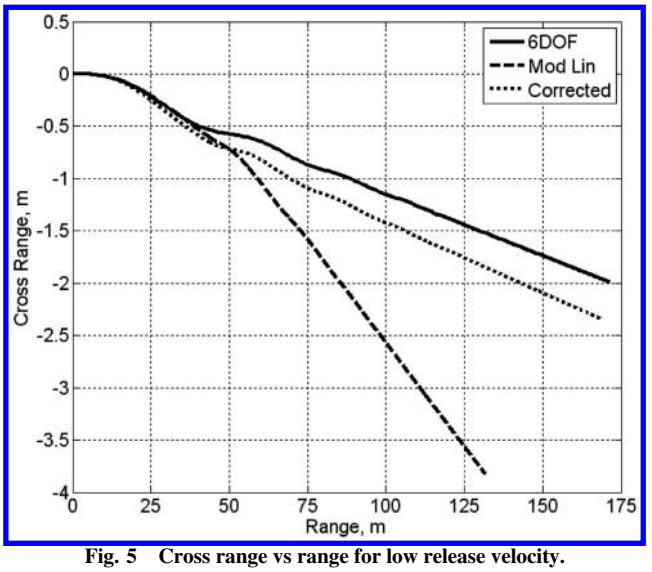

Fig. 5 Cross range vs range for low release velocity.

Altitude and cross range are shown in Figs. 4 and 5, in which it is clear that modified linear theory fails to predict the impact location accurately. Modified linear theory results in impact-prediction errors of 40 and 1.9 m in range and cross range, compared with 3.4 and 0.4 m for low-speed linear theory. Errors in range and cross range from modified linear theory result mainly from large errors in Euler angles, which are significantly less for low-speed linear theory. Errors in angle predictions are smaller in low-speed linear theory due to the point-mass-velocity assumption and the addition of considering $\tilde{w}$ and $\tilde{q}$ as having significant contributions. Low-speed linear theory also reduces impact-prediction error by including $\tilde{w}$ directly into the cross-range equation, as seen in Eq. (25).

V. Predictive Control System

The predictive control system uses low-speed modified linear theory to predict the impact location based on the current munition states, constant pitch and yaw moment commands, and target altitude. The predicted impact location defined by x_I and y_I is compared with the target locations x_T and y_T to generate errors in the range and cross range at impact. The control system seeks to minimize the penalty function in Eq. (54) using the two control parameters in Eq. (56), subject to the constraint that the magnitude of each element of the control vector $\mathbf{u}$ is bounded by $C_{\max}$.

$$J = \mathbf{e}^T\mathbf{e} \tag{54}$$

$$\mathbf{e} = \{\,(x_I - x_T) \quad (y_I - y_T)\,\}^T \tag{55}$$

$$\mathbf{u} = \{\,C_{MM} \quad C_{NN}\,\}^T \tag{56}$$

The penalty function in Eq. (54) is a nonlinear function of all the munition states and the two control elements with no closed-form solution available. An approximate numerical solution can be found by using the rapid impact-prediction capabilities of low-speed linear theory and a gradient descent method [15]. Figure 6 shows a diagram of the complete predictive control system. First, the approximate optimal control vector $\mathbf{u}^*$ is initialized to zero. The current munition state vector is measured and low-speed linear theory is used to predict the impact error $\mathbf{e}$. A perturbation to the current control is found by multiplying a 2×2 matrix K by the current impact error. To satisfy the constraint, the perturbed control vector is then saturated with respect to $C_{\max}$. The control vector continues to be updated until either $\|\mathbf{e}\| \leq e_{\max}$ or the maximum iterations $k_{\max}$ occur. The approximate optimal control is applied and the process is repeated at the next measurement update, starting with the previous approximate

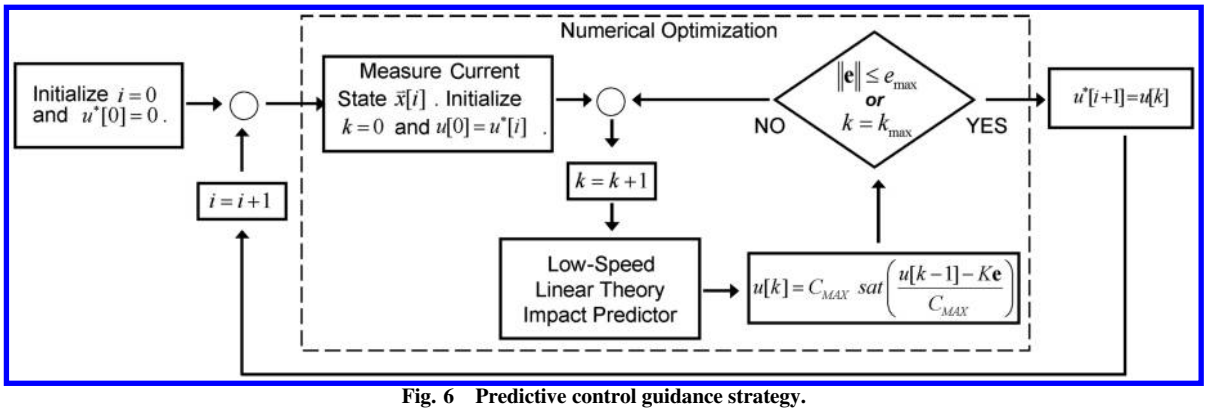

Fig. 6 Predictive control guidance strategy.

optimal solution. For a fin-stabilized munition with zero roll, the impact range and cross range will increase for positive control coefficients C_{MM} and C_{NN}, requiring K to be positive definite. A simple proportional–derivative roll controller is used to regulate the roll angle after release and is provided in Eq. (57).

$$C_{LL} = K_\phi \phi + K_p \tilde{p} \tag{57}$$

Typical guided trajectories of the example 40-mm grenade with tail section are shown in Figs. 7–10 for $k_{\max}$ of 1 and 10. When $k_{\max}$ is 1, the numerical solution for $\mathbf{u}^*$ is stopped after just one application of the low-speed linear theory predictor, resulting in a rapid solution at the expense of accuracy. The grenade is released with the following initial conditions: $x = -180$ m; $y = 10.0$ m; $z = 500$ m; ϕ, θ, ψ, $\tilde{v}$, $\tilde{w}$, and $\tilde{p} = 0.0$ deg; $\tilde{u} = 20.0$; $\tilde{q} = -0.15$ rad/s; and $\tilde{r} = -0.15$ rad/s. The possible singularity when θ is $\pm\pi/2$ is avoided by stepping to either side by 0.01 rad if it occurs. The desired target is x_T, y_T, and $z_T = 0$ m. The control system is updated every 0.5 s with the low-speed linear theory impact predictor using an update interval of 250 calibers. The perturbation matrix K is chosen as diagonal with 0.00005 elements, the saturation limit $C_{\max}$ is 0.0015, $e_{\max}$ is 1.0 m, and the roll gains K_ϕ and K_p are -0.125 and -0.01. Figure 7 shows the altitude vs range and Fig. 8 shows the cross range. In both Figs. 7 and 8, the trajectories for $k_{\max}$ of 1 and 10 are nearly indiscernible. Figure 9 shows the control history for both guided trajectories and the number of iterations used in the numerical solution. Initially, when $k_{\max}$ is large, multiple iterations are used. However, after 1.5 s, control trajectories for $k_{\max}$ of both 1 and 10 are nearly identical. Figure 10 shows a history of the low-speed linear theory impact prediction, with the square and circle representing the impact of the unguided and guided grenade, respectively. At release, when $k_{\max}$ is 10, multiple iterations of the low-speed impact predictor are use to estimate $\mathbf{u}^* = [\,0.0011 \quad -0.00075\,]^T$, which is near the final solution at impact. The approximate $\mathbf{u}^*$ calculated at release results in a predicted impact close to the target. During the next eight measurement updates, controls are slightly modified, reaching a near-constant solution within 5 s. At all times, the predicted impact is

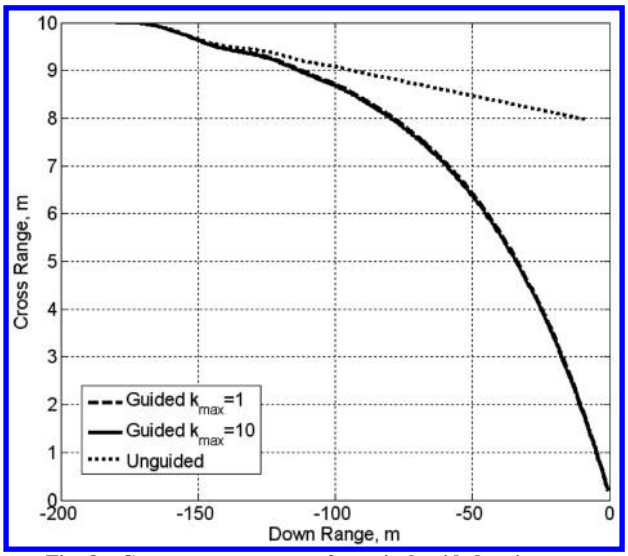

Fig. 8 Cross range vs range of a typical guided trajectory.

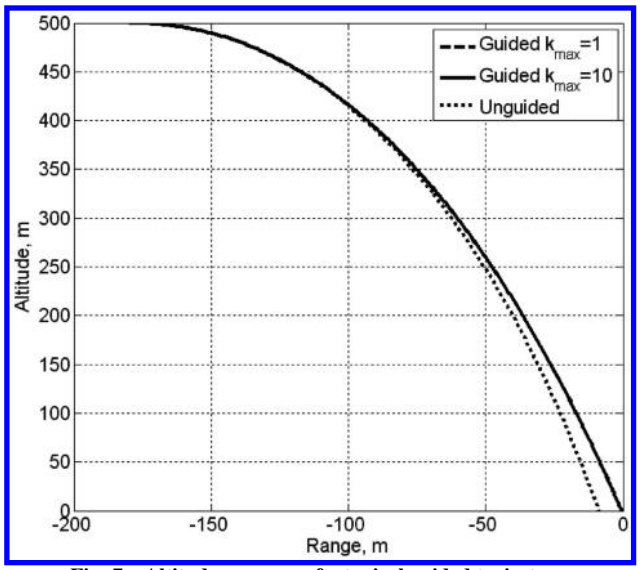

Fig. 7 Altitude vs range of a typical guided trajectory.

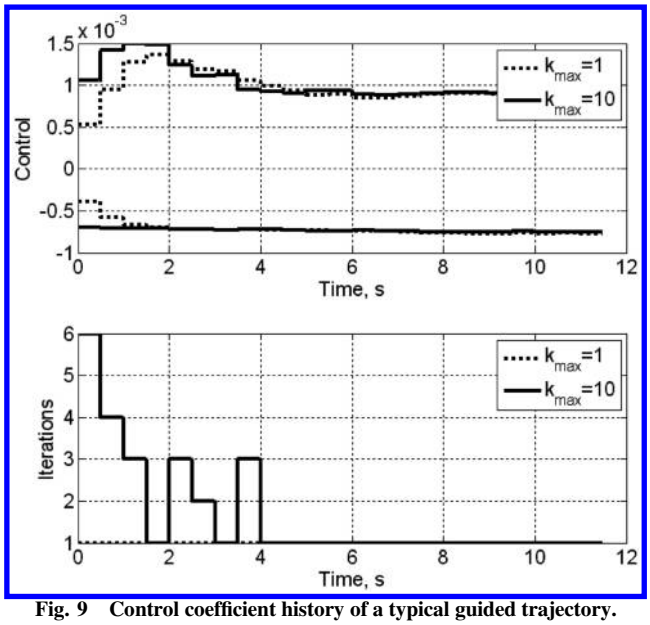

Fig. 9 Control coefficient history of a typical guided trajectory.

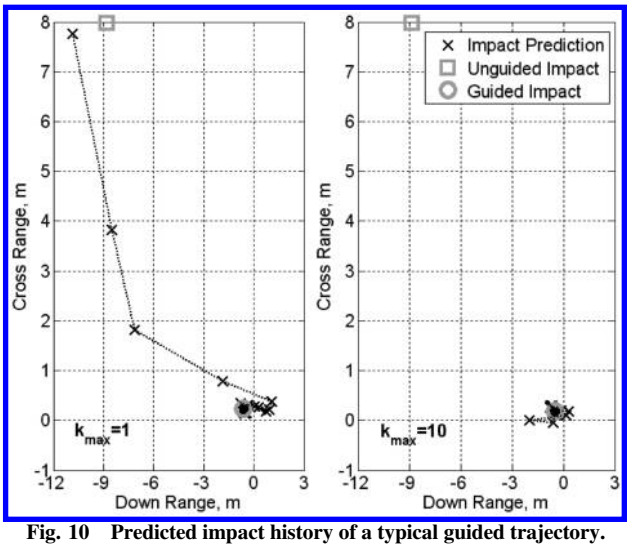

Fig. 10 Predicted impact history of a typical guided trajectory.

near the desired impact. For $k_{\max}$ equal to 1, the impact prediction at release is near the unguided impact. During the next four control updates, the predicted impact continually moves closer to the desired impact location. With $k_{\max}$ equal to 1, the predictive control still successfully placed the grenade on a correct trajectory within 5 s. The predictive controller reduces impact error from 11.9 m for the unguided grenade to 0.6 and 0.5 m for the guided grenade, with $k_{\max}$ being 1 and 10, respectively.

Monte Carlo simulations were completed for the unguided and guided example grenade, with $k_{\max}$ being 1 and 10. Dispersion results are shown in Fig. 11 for 50 trajectories. The release position is nominally $x = -170$ m, $y = 0.0$ m, and $z = 500$ m, with each position independently varied, having a Gaussian distribution with standard deviation of 5.0 m. Release speeds $\tilde{u}$ and $\tilde{v}$ are independently varied, having means of 20 m/s and 0 m/s and Gaussian distributions with standard deviations of 1.0 m/s. Initial angular rates $\tilde{q}$ and $\tilde{r}$ are also independently varied, having means of 0 rad/s and standard deviations of 0.1 rad/s. All other initial conditions are zero. A constant atmospheric wind is included for each

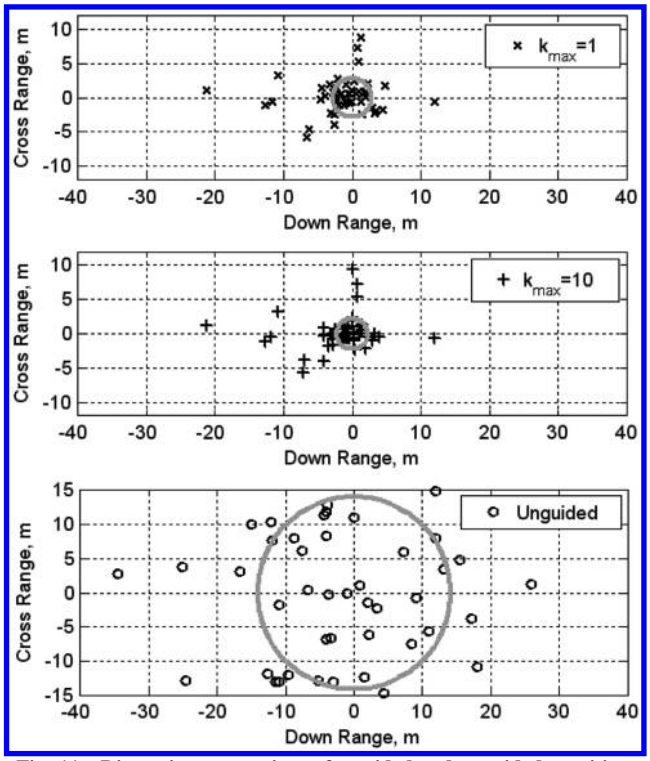

Fig. 11 Dispersion comparison of a guided and unguided munition.

release; however, the control algorithm has no knowledge of the wind and assumes they are zero during impact prediction. The wind magnitude varies with a standard deviation of 3.0 m/s and the direction is uniformly distributed. Gaussian noise is added to the control system sensors, with a standard deviation of 1.0 m on x, y, and z; a standard deviation of 0.018 rad on ϕ, θ, and ψ; a standard deviation of 0.15 m/s on $\tilde{u}$, $\tilde{v}$, and $\tilde{w}$; and a standard deviation of 0.018 rad/s on $\tilde{p}$, $\tilde{q}$, and $\tilde{r}$. The circular error probable (CEP) is shown in Fig. 11 and is defined as the minimum radius circle containing 50% of the hits. The predictive control algorithm shows a drastic improvement in dispersion, reducing the CEP from 14.1 to 2.7 and 2.2 m for $k_{\max}$ equal to 1 and 10. It is worth noting that a standard high-explosive 40-mm grenade such as the M460 has a burst radius that causes casualties within 5 m. For the unguided grenade, only 10% of impacts are within 5 m, whereas for both $k_{\max}$ equal to 1 and 10, the predictive guidance increases impacts within 5 m to 78%.

VI. Conclusions

Modified linear theory provides reasonable impact predictions at high speeds. However, for typical small UAS mission speeds, less than 20-m/s impact errors were substantial due to large angles of attack and pitch rates. Low-speed linear theory was developed by including higher-order terms involving $\tilde{w}$ and $\tilde{q}$ that modified linear theory neglects. As a result, the angle of attack, pitch, and yaw predictions are significantly improved, leading to accurate impact predictions even at very low speeds.

A predictive control scheme was developed to reduce dispersion using control surfaces near the tail. The predictive controller uses low-speed linear theory to rapidly predict the impact error using the current state and control. Based on the estimated impact error, the control is iteratively found to minimize the predicted-impact error. For an example munition, it was shown that the maximum number of iterations during the control solution only impacted the initial control estimates. Limiting the guidance algorithm to a single iteration had little impact on the final accuracy and permitted a rapid solution. It was shown for the example munition that the predictive guidance significantly reduced the CEP from 14.1 to 2.7 and 2.2 m when the maximum iterations were 1 and 10. Furthermore, for a typical high-explosive 40-mm grenade, the percentage of impacts within a lethal radius was increased from 10 to 78% when the maximum iterations were both 1 and 10. In practical applications, errors in the target location must be included when considering the probability of impact within a lethal range of a target.

References

[1] Zarchan, P., *Tactical and Strategic Missile Guidance*, AIAA, Reston, VA, 1997, pp. 11–28, 95–118, 185–205.

[2] Calise, A., "An Analysis of Aerodynamic Control for Direct Fire Spinning Projectiles," AIAA Paper 2001-4217, Aug. 2001.

[3] Jitpraphai, T., and Costello, M., "Dispersion Reduction of a Direct Fire Rocket Using Lateral Pulse Jets," *Journal of Spacecraft and Rockets*, Vol. 38, No. 6, 2001, pp. 929–936.

[4] Calise, A., Sharma, M., and Corban, J., "Adaptive Autopilot Design for Guided Munitions," *Journal of Guidance, Control, and Dynamics*, Vol. 23, No. 5, 2000, pp. 837–843.

[5] Curtis, J., "An Input-to-State Stabilizing Control Lyapunov Function for Autonomous Guidance and Control," AIAA Paper 2005-6282, Aug. 2005.

[6] Slegers, N., and Costello, M., "Model Predictive Control of a Parafoil and Payload System," *Journal of Guidance, Control, and Dynamics*, Vol. 28, No. 4, 2005, pp. 816–821.

[7] Slegers, N., Kyle, J., and Costello, M., "A Nonlinear Model Predictive Control Technique for Unmanned Air Vehicles," *Journal of Guidance, Control, and Dynamics*, Vol. 29, No. 5, 2006, pp. 1179–1188. doi:10.2514/1.21531

[8] Burchett, B., and Costello, M., "Model Predictive Lateral Pulse Jet Control of an Atmospheric Rocket," *Journal of Guidance, Control, and Dynamics*, Vol. 25, No. 5, 2002, pp. 860–867.

[9] Ollerenshaw, D., and Costello, M., "Model Predictive Control of a Direct Fire Projectile Equipped with Canards," AIAA Paper 2005-5818, Aug. 2005.

[10] McCoy, R., *Modern Exterior Ballistics*, Schiffer, Attlen, PA, 1999, pp. 221–244.

[11] Murphy, C., "Angular Motion of a Spinning Projectile with a Viscous Fluid Payload," *Journal of Guidance, Control, and Dynamics*, Vol. 6, No. 4, 1983, pp. 280–286.

[12] Cooper, G. R., and Costello, M., "Flight Dynamic Response of Spinning Projectiles to Lateral Impulsive Loads," *Journal of Dynamic Systems, Measurement, and Control*, Vol. 126, Sept. 2004, pp. 605–613. doi:10.1115/1.1789976

[13] Costello, M., and Peterson, A., "Linear Theory of a Dual-Spin Projectile in Atmospheric Flight," *Journal of Guidance, Control, and Dynamics*, Vol. 23, No. 5, 2000, pp. 789–797.

[14] Hainz, L. C., III, and Costello, M., "Modified Projectile Linear Theory for Rapid Trajectory Prediction," *Journal of Guidance, Control, and Dynamics*, Vol. 28, No. 5, 2005, pp. 1006–1014.

[15] Stengel, R. F., *Optimal Control and Estimation*, Dover, New York, 1994, pp. 254–270.